Science of the Total Environment 903 (2023) 166572

Contents lists available at ScienceDirect

Science of the Total Environment

journal homepage: www.elsevier.com/locate/scitotenv

# Thermal impact of underground car parks on urban groundwater

Maximilian Noethen [a,*], Hannes Hemmerle [a], Kathrin Menberg [b], Jannis Epting [c], Susanne A. Benz [d], Philipp Blum [b], Peter Bayer [a]

[a] Department of Applied Geology, Institute of Geosciences and Geography, Martin Luther University Halle-Wittenberg, Germany
[b] Institute of Applied Geosciences (AGW), Karlsruhe Institute of Technology (KIT), Germany
[c] Applied and Environmental Geology, Hydrogeology, Department of Environmental Sciences, University of Basel, Switzerland
[d] Institute of Photogrammetry and Remote Sensing (IPF), Karlsruhe Institute of Technology (KIT), Germany

## HIGHLIGHTS

- Underground car parks are major contributors to urban subsurface warming.
- Time series analysis shows seasonal variation of heat flux intensity and direction.
- Upscaling of the thermal impact to city-scale by multiple linear regression.
- Highest heat fluxes occur where the groundwater is shallow and cool.
- Harnessing waste heat can provide green energy and reduce the impact on groundwater.

## GRAPHICAL ABSTRACT

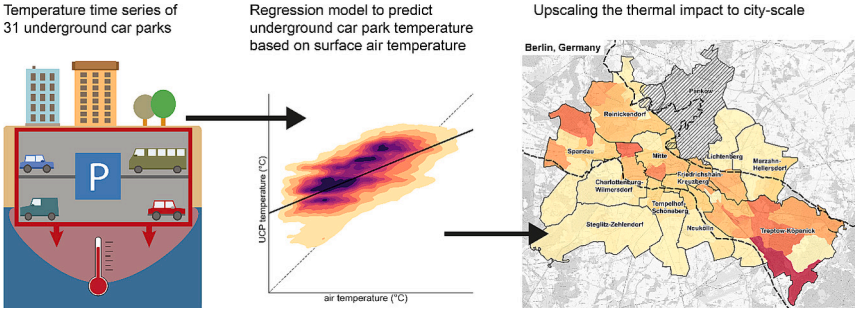


## ARTICLE INFO

Editor: Jurgen Mahlknecht

*Keywords:*
Heat source
Anthropogenic heat flux
Subsurface urban heat island
Groundwater temperature
Urban hydrology
Underground parking

## ABSTRACT

Built-up areas are known to heavily impact the thermal regime of the shallow subsurface. In many cities, the answer to densification is to increase the height and depth of buildings, which leads to a steady growth in the number of underground car parks. These underground car parks are heated by waste heat from car engines and are typically several degrees warmer than the surrounding subsurface, which makes them a heat source for ambient subsurface and groundwater. Thus, the objective of this study is to investigate the thermal impact of 31 underground car parks in six cities and to upscale the thermal impact that underground car parks have on the subsurface in Berlin, Germany. Underground car parks have daily, weekly, and seasonal temperature patterns that respond to air circulation and traffic frequency, resulting in net heat fluxes of 0.3 to 15.5 W/m$^2$ at the measured sites. For the studied underground car parks in Berlin, the emitted annual thermal energy is about 0.65 PJ. Recycling this waste heat with geothermal heat pumps would provide a sustainable alternative for green energy and counteract the urban heat island by cooling of the shallow subsurface.

## 1. Introduction

Groundwater is highly important not only as our largest available freshwater resource but also because it provides an extensive habitat for subsurface ecosystems that are valuable to our society (Boulton et al., 2008; Griebler and Avramov, 2015; Hancock et al., 2005). Due to their

* Corresponding author.
*E-mail address:* maximilian.noethen@geo.uni-halle.de (M. Noethen).

https://doi.org/10.1016/j.scitotenv.2023.166572
Received 4 April 2023; Received in revised form 3 August 2023; Accepted 23 August 2023
Available online 24 August 2023

purification function, a deterioration of groundwater ecosystems could lead to a decrease in groundwater quality (Bonte et al., 2011; Brielmann et al., 2009). For sustainable cities, it is therefore necessary to protect these vulnerable ecosystems. In addition to various other anthropogenic influences such as salt pollution and organic chemicals (Becher et al., 2022), temperature increase is assumed to pose a threat to groundwater fauna (Griebler et al., 2016). Thus, changing groundwater temperatures in cities lead to a decline in the biodiversity of fauna and can affect groundwater quality (Blum et al., 2021; Koch et al., 2020; Spengler and Hahn, 2018). Furthermore, a temperature increase in the shallow subsurface can lead to increased temperatures in drinking water distribution systems (Agudelo-Vera et al., 2017; Gunkel et al., 2022). Especially in urban areas, they are often installed close to underground infrastructure and therefore directly affected (van den Bos, 2020). Exceeding recommended temperature limits of 20 to 25 °C can result in bacterial growth in drinking water (Agudelo-Vera et al., 2020).

Temperatures in the urban environment are altered by various anthropogenic sources. So-called urban heat islands indicate increased air temperatures in cities (Oke, 1973). The same observation has been made for the subsurface. Due to a number of different heat sources, such as basements, tunnels, and surface sealing (Attard et al., 2016; Noethen et al., 2022; Tissen et al., 2021), groundwater temperatures beneath cities are permanently elevated, which is typically referred to as subsurface urban heat island (Ferguson and Woodbury, 2004; Hemmerle et al., 2022; Menberg et al., 2013a; among others). In general, temperatures scale with building density and in urban centers, increased groundwater temperatures of up to 7 K can be observed (Böttcher and Zosseder, 2022; Menberg et al., 2013a). In historical cities, such anomalies can be traced to depths of >60 m below the surface, proving that regional subsurface warming went along with urban expansion in the past (Visser et al., 2020). Intensities and drivers of urban subsurface warming have been intensively studied (Benz et al., 2018; Menberg et al., 2013b) as has the exploration of accumulated waste heat as a geothermal resource (Benz et al., 2022; Menberg et al., 2015; Tissen et al., 2021). Nevertheless, there is a lack of knowledge about the characteristics of heat sources and their impact in the context of an urban environment. Especially in the densest agglomerations, it is difficult to distinguish between individual heat sources as their effects overlap and add up to regional scale thermal anomalies.

Within European inner-city settings, these heat sources typically include a large number of underground car parks (UCP). They have been observed in association with hot spots in groundwater temperatures (Becker and Epting, 2021; Zhu et al., 2015). However, UCPs are often generalized as basements (e.g. Benz et al., 2015; Menberg et al., 2013b), underground structures (Attard et al., 2016), or subsurface buildings (Epting et al., 2017b). This ignores that UCPs, in comparison to regular basements, extend over several levels and, although typically not insulated, are passively heated by traffic (Becker and Epting, 2021). For these reasons, UCPs can be more effective heat sources than basements (Noethen et al., 2022). Becker and Epting (2021) directly addressed UCPs as heat sources and found that public UCPs have higher temperatures than private ones due to higher traffic volumes. Rotta Loria et al. (2022) found a positive linear relationship between air and UCP temperatures. UCP air tends to be warmer than surface air in winter and cooler in summer.

Although it is proven that UCPs can create local hot spots, their overall contribution to urban subsurface warming has not been sufficiently investigated yet. To overcome this gap the first objective of this study is to evaluate the thermal state of 31 UCPs in Central Europe with respect to (i) ambient air temperature, (ii) the usage type and traffic load of the UCP, and (iii) the thermal impact they have on groundwater. The second objective is to use the information gained by the reference underground car parks to upscale the thermal impact at the city-scale for Berlin. We perform a spatial and temporal analysis to assess heat fluxes of 5040 UCPs in Berlin and present the contribution of UCPs to urban subsurface warming.

## 2. Materials and methods

### 2.1. Underground car park temperatures

#### 2.1.1. Monitoring sites and data

The monitored UCPs are located in major cities in Germany, Austria, and Switzerland. We investigate ten UCPs in Cologne (Cologne #1 to #10), one in Halle and one in Karlsruhe, twelve in Vienna (Vienna #1 to #12), five in Basel (Basel #1 to #5), and two in Zürich (Zürich #1 and #2) (Fig. 1). The exact location of the UCPs is not disclosed for data protection reasons.

The data used for the temperature analysis include time series of air temperature in the UCPs ($T_{UCP}$), air temperature outside the UCP ($T_{Air}$), and groundwater temperature ($T_{GW}$), where available. For six sites with nearby groundwater observation wells, temperature-depth-profiles, measured between 2013 and 2022, were also available. We also recorded information on the depth of the UCP and the type of use (private/public). Information and sources of all datasets are given in Table A1. The measurement of $T_{UCP}$ was carried out in several field campaigns, over several years (2014–2022) and with varying equipment and personnel. Hence, there are variations in the placement of the device and in the accuracy and resolution of the data. However, all the devices used have a minimum accuracy of ±0.5 K and a minimum resolution of 0.1 K.

$T_{Air}$ data were obtained from the nearest available weather station for each UCP. Due to the differences in microclimatic conditions between weather station and UCP, $T_{Air}$ could deviate from the true value. For example, in some cities such as Cologne or Karlsruhe, the weather station is positioned outside of the city, where $T_{Air}$ is typically cooler than in the city center. This can cause an error (see Fig. A1 for Berlin as example). $T_{GW}$ data were obtained from authorities or by own measurements. At Zürich #1 and Zürich #2 $T_{GW}$ was measured directly below the UCP in wells located inside the buildings on the first and second level, respectively.


**Fig. 1.** Map of the study sites. Cities with studied UCP sites are indicated by dots. Berlin is represented by the city area.

#### 2.1.2. Data analysis

The workflow for determining the heat fluxes from the measured UCPs into the groundwater and the linear regressions is shown in Fig. 2 in the left part.

The vertical conductive heat transport from the UCP through the slab into the groundwater was calculated as follows:

$$q_{slab} = U \cdot \Delta T \quad (1)$$

where $q_{slab}$ is the heat flux through the slab in W/m$^2$, which quantifies the rate of heat transfer per unit area, $\Delta T$ is the difference between $T_{UCP}$ and $T_{GW}$ in K, and $U$ is the thermal transmittance in W/(m$^2$·K). The thermal transmittance measures the heat transfer through solid matter between two fluids and is derived from the reciprocal value of the thermal resistance ($R$):

$$U = \frac{1}{R} \quad (2)$$

The thermal resistance indicates the resistance of a material or structure to heat flow and is calculated according to the following formula (DIN EN ISO 6946, 2018):

$$R = \frac{1}{\alpha} + \frac{d_{slab}}{\lambda_{concrete}} + \frac{d_{soil}}{\lambda_{soil}} \quad (3)$$

This equation adds up the resistances of every permeated layer, which in this case are the slab of the UCP and the unsaturated soil beneath. The thermal resistance of each layer is obtained by dividing the permeated layer's thickness ($d$) and its thermal conductivity ($\lambda$). Nowadays, UCPs are typically built with spread foundations with a thickness between 0.4 and 0.6 m. Older UCPs also have strip foundations, where deeper foundations were constructed in trenches and a thinner slab of 0.2 to 0.25 m carries only the load of the cars. Since there is no information about the age of construction, we assumed for all UCPs spread foundations with $d_{slab}$ = 0.5 m. Unsaturated soil thickness was derived from the distance between the UCP base and local groundwater tables. For the thermal conductivity of the concrete and the soil, typical values were chosen based on VDI 4640 (2010) and the geology of the soil (see Table A2). For the UCPs that reach the groundwater, only the thermal resistance of the slab was calculated. Furthermore, the reciprocal value of the heat transfer coefficient ($\alpha$) is added. This value, which integrates the energy transfer between concrete and air inside the UCP, was adopted from Guo et al. (2011), assuming a low wind velocity in UCPs of 0.1 m/s: $\alpha$ = 8.75 W/m$^2$·K. The resulting reciprocal value is 0.114 W/m$^2$·K, which is slightly lower than the standard value for the inner surface resistance of 0.13 W/m$^2$·K by DIN EN ISO 6946 (2018). We prefer this experimental value of Guo et al. (2011) because it additionally considers wind velocity. In UCPs, there is typically either a natural or a mechanical ventilation system because of car exhaust fumes, as required by law in many countries (e.g., §11 GaVo, 2022). In Eq. (1), $\Delta T$ was calculated temporally resolved to consider seasonal fluctuations. For Zürich #1 and Zürich #2, no groundwater time series was available. Instead, we used the mean of all temperature-depth-profiles at 20 m below ground surface (bgs) as a constant value.

For the correlation of $T_{UCP}$ and $T_{Air}$, we used the Pearson correlation coefficient ($r$). The average linear regression and correlation coefficient per level was calculated with the mean values of the individual sites of the respective levels and the total regression with the mean values of all sites. No average regression was calculated for levels five and six since there is only one UCP representing each of these levels.

### 2.2. Impact of underground car parks on subsurface warming of Berlin

#### 2.2.1. Study area

For the spatial analysis of heat fluxes from UCPs, we chose the city of

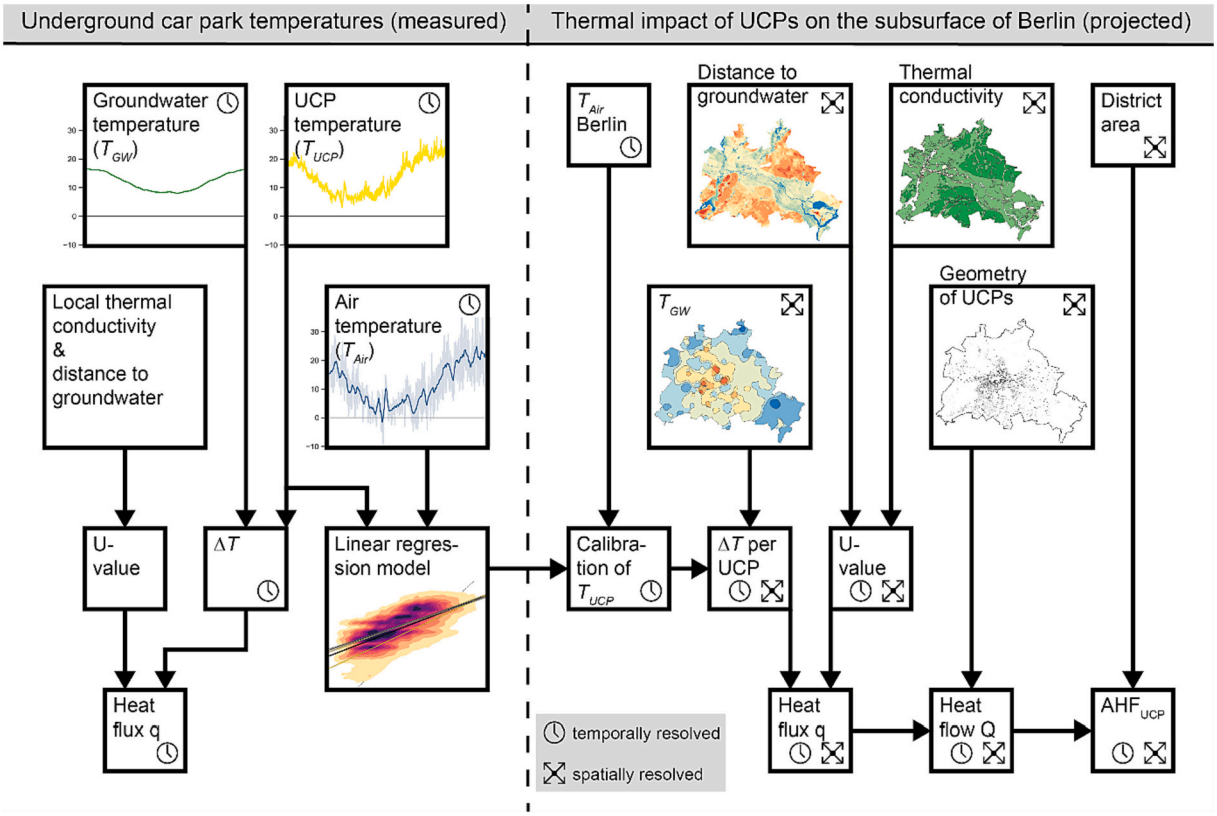


**Fig. 2.** Workflow chart of the calculation of heat fluxes from the measured UCPs (left) as well as the heat fluxes and heat flows for UCPs in Berlin and the anthropogenic heat flux of UCPs ($AHF_{UCP}$) per district (right). Detailed versions of the maps on the right can be seen in Fig. A2. $\Delta T$: temperature difference, U-value: thermal transmittance.

Berlin as case study site, because it offers a well-curated open data service and has a large number of UCPs in different geological settings. With >3.5 million inhabitants and an area of 891.1 km$^2$, Berlin is Germany's largest city and capital. The district of Pankow was excluded due to a lack of data at this specific location. Parts of the districts of Reinickendorf and Mitte were also excluded because there is no shallow aquifer in these areas and therefore no meaningful distance to the groundwater can be calculated (Geoportal Berlin, 2023). The arithmetic mean of $T_{Air}$ at the weather station of Berlin-Tempelhof between 1990 and 2021 is 10.4 ± 0.8 °C (DWD, 2023). The city is located in a transitional climate zone between maritime and continental influences. However, Berlin's climate is also strongly influenced by anthropogenic land use and forms an urban heat island. The average $T_{Air}$ is between 1.5 and 2 K warmer than in the surrounding rural areas (Vogel and Afshari, 2020; Ward et al., 2016).

The shallow subsurface of north-eastern Germany was shaped by glacial periods and the morphology of Berlin was primarily by the Weichselian glaciation. The Warsaw-Berlin glacial valley cuts from southeast to northwest through the Barnim and Teltow plateaus, which are located in northeast and southwest Berlin. The valley, which hosts the Spree River today, consists mainly of glacial and fluvial sands, while the plateaus are mainly built up of glacial till and sand (Geoportal Berlin, 2023).

The hydrogeology in Berlin is complex due to the glacial genesis; several aquifers are separated by aquitards (Limberg and Thierbach, 1997). The groundwater level in the glacial valley, where the city center is located, is <10 m bgs in most parts. On the plateaus, the distance to the groundwater table is 10 to 40 m bgs, except for some morphological depressions, where it can be less (Hannappel and Limberg, 2007). $T_{GW}$ is highest in the central parts (~14 °C) and decreases with distance from the city center, thus forming the typical subsurface urban heat island (Menberg et al., 2013a). At the outer parts, $T_{GW}$ was found to be around 10 to 11 °C (Geoportal Berlin, 2023).

#### 2.2.2. Input data

For the spatial analysis of heat fluxes, the most recent datasets which are freely accessible via the online open data portal of Berlin were used (Geoportal Berlin, 2023):

- $T_{GW}$ of 2020 at 20 m bgs interpolated from 223 wells.
- Depth to the groundwater table for May 2009 interpolated from 1750 wells.
- Geological sketch of the surface lithology, based on various geological maps.
- Geometry of buildings in Berlin including information about the geometry of the UCPs and the number of subsurface levels. The height of the UCP levels is assumed to be 3 m.
- District and city quarter area.

The thermal conductivity of the soil was derived from the surface lithology data of the geological sketch using literature values (VDI 4640, 2010). For the soil, the average value between dry and moist material was used (for till and peat the recommended value, for concrete 1.6 W/m·K). For the building dataset, we expect that a small fraction of the private UCPs is not registered at the municipality and that the actual number of UCPs in the study area is even higher. The spatial datasets applied in the calculation are shown in Fig. A2.

$T_{UCP}$ is derived from $T_{Air}$ by the linear regressions from own measurements at 31 UCPs for each level. $T_{Air}$ was calculated as monthly long-term averages (1990–2021) with data from the DWD (2023), measured at the Berlin-Tempelhof weather station (location shown in Fig. A2d). The UCPs are distributed over the entire area of Berlin and, due to the size of the city, they can be up to 23 km away from the weather station. The urban heat island effect likely affects the $T_{Air}$ data used in this approach (Dugord et al., 2014; Kottmeier et al., 2007) and microclimatic variations in the study area are not considered. Comparing the other weather stations in Berlin to the one in Berlin-Tempelhof, the annual mean $T_{Air}$ deviation is always <1 K (see Fig. A1). Therefore, we can assume a maximum error of ±1 K for $T_{Air}$.

All input parameters applied in the spatial analysis are listed in Table A2.

#### 2.2.3. Spatial analysis

In order to extrapolate the thermal impact of UCPs to the city-scale, we projected the results from the UCP temperature analysis of the measured sites on all UCPs in Berlin (Fig. 2, right part). For each UCP in the study area, we calculated the heat flux through the slab using Eqs. (1)–(3). For the UCPs that reach into the groundwater, heat transfer of all walls below the water table is determined. The heat flux through the walls in the unsaturated soil can be neglected as most of the heat escapes to the surface (Emery et al., 2007; Thomas and Rees, 1999). The heat flux through the wall is calculated only using the resistance of the concrete as there is no soil obstructing the heat flow into the groundwater. We assumed a wall thickness of 0.3 m, which results from the typically used 0.25 m wide sheet metal strips with additional concrete cover. The mean heat flux through the slab and wall per district is calculated as a weighted mean with the heat flux and area of the individual UCPs.

Furthermore, we calculated the heat flow ($Q$) from the UCP into the groundwater as follows:

$$Q = q_{slab} \cdot A_{UCP} + q_{wall} \cdot A_{wall} \quad (4)$$

where $A_{UCP}$ is the area of the slab and $A_{wall}$ is the area of the walls inside the groundwater.

Consequently, we determined the anthropogenic heat flux that is emitted into the shallow urban aquifer by various anthropogenic sources (Benz et al., 2015; Menberg et al., 2013b). In this case, we calculated the anthropogenic heat flux of UCPs ($AHF_{UCP}$) in Berlin, normalized to the area of the district ($A$):

$$AHF_{UCP} = \sum q \cdot A_{UCP} \Big/ A \quad (5)$$

## 3. Results and discussion

### 3.1. Underground car park temperatures

#### 3.1.1. Thermal impact on groundwater

UCPs are known to cause warming of the surrounding soil and groundwater (Becker and Epting, 2021; Zhu et al., 2015). Fig. 3 shows temperature logs measured at groundwater monitoring wells inside a public (Zürich #1) and a private UCP (Zürich #2). Both UCPs have a well inside the building, Zürich #1 at the first level, Zürich #2 at the third level. Since the groundwater tables are higher than the UCP foundations, $T_{GW}$ can be measured at the depths of the lower levels. Zürich #1 shows a significant influence on $T_{GW}$ due to the high $T_{UCP}$. The heat comes from above, which is reflected in the warm $T_{GW}$ at the upper meters. Only in the winter months, when $T_{UCP}$ is colder than $T_{GW}$, there is no heating effect. The $T_{GW}$ at 20 m bgs is 16.6 °C and 2.7 K cooler than the average $T_{UCP}$. It should be noted that the third level is used as a nuclear shelter and no cars are parked there. In comparison, Zürich #2 is a private car park with more levels. Similar to Zürich #1, the levels three and four are reserved as a nuclear shelter without traffic. Although $T_{GW}$ in the top five meters below the structure is slightly warmer in summer and autumn, there is no significant influence over the course of the year. $T_{GW}$ at 20 m bgs is 13.7 °C and 1.8 K cooler than the average $T_{UCP}$. This indicates that there is still a heating effect on the groundwater due to the thermal gradient between the UCP and the groundwater, however, it is not as pronounced as at Zürich #1.

As indicated by the seasonal variance of the temperature logs at Zürich #1 and #2 the heat flux is depending on seasonal variations of both $T_{UCP}$ and $T_{GW}$. Fig. 4 shows a time series of $T_{GW}$, $T_{UCP}$, $T_{Air}$, as well

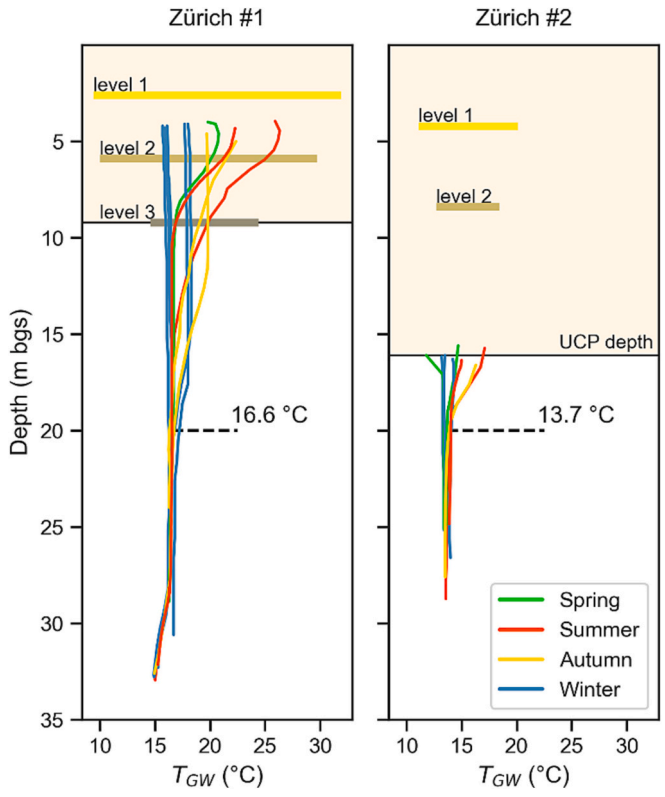


**Fig. 3.** Temperature-depth-profiles of a public (Zürich #1) and a private UCP (Zürich #2), measured in observation wells inside the UCP. At the top, the UCP temperature range per level is shown with a bar, while the average groundwater temperature at 20 m bgs is indicated with a dashed line.

as the heat fluxes over time and as boxplots for each site based on the observed temperature data. The heat fluxes show different patterns and variate in intensity and even direction throughout the seasons. Zürich #1 shows that $T_{UCP}$ in the upper two levels responds rapidly to $T_{Air}$, which indicates a good connection to surface air. In Zürich #2, the opposite can be observed. Here, $T_{UCP}$ hardly responds to $T_{Air}$. The high heat fluxes at both sites in Zürich can be attributed to the direct connection of the UCPs to the groundwater. $T_{UCP}$ of Basel #4 is higher in all seasons than $T_{GW}$. The UCP is surrounded by groundwater and has the largest impact on the groundwater of the studied UCPs, with an average heat flux of 15.5 ± 3.3 W/m$^2$. The development of temperatures at Basel #5 is similar to those of Basel #4, and its base is also in the saturated zone, but the surrounding groundwater is 4.1 K warmer on average. This results in a smaller mean heat flux of 4.3 ± 6.3 W/m$^2$ and a reverse of the flux direction in winter and spring seasons. Although the UCP Cologne #8 is considerably warm with an average $T_{UCP}$ of 19 ± 3.2 °C, no significant net heat flux into the groundwater occurs (mean 0.3 ± 0.5 W/m$^2$). This can be attributed to the already high $T_{GW}$ (17 ± 0.4 °C) and higher distance to the groundwater (6 m below the UCP base). In contrast to the publicly used UCPs, the shallow and privately used UCP in Halle is well connected to the surface air and therefore only 1.4 K warmer than the groundwater on average. Although groundwater is found only 0.5 m below the structure, the UCP has almost no thermal impact (1.4 ± 6.2 W/m$^2$). Overall, mean heat flux intensities ranging between 0.3 and 15.5 W/m$^2$ are highly sensitive to the distance to the groundwater and pre-altered thermal groundwater conditions. Furthermore, the variation in the placement of the device may impact the results as temperatures within the same level can vary. In Fig. A4, we show the high relevance of $T_{UCP}$ to the results, as this parameter has the highest sensitivity.

### 3.1.2. Correlation of UCP and air temperature

The relationship between $T_{UCP}$ and $T_{Air}$ for the six individual UCPs with $T_{GW}$ information is shown in Fig. 5. Furthermore, the mean for all 31 monitored UCPs is plotted at the bottom of the figure. Scatter plots for all individual sites are given in the appendix in Fig. A3. All sites exhibit a positive linear correlation with weaker correlation coefficients and lower gradients at deeper UCP levels. This indicates that the influence of $T_{Air}$ (e.g., through ventilation) decreases with increasing depth. For example, at the deepest levels in the UCPs Basel #4 at 10 m bgs and #5 at 16 m bgs seasonal variation of $T_{UCP}$ is negligibly low with a seasonal amplitude below 5.8 and 9.2 K, respectively, whereas the seasonal amplitude of $T_{Air}$ is 29.6 K. In 84.9 % of all data pairs, $T_{UCP}$ is warmer than $T_{Air}$, which is represented by values above the dashed identity line. However, some UCPs appear to be better connected to the surface air and show a weaker deviation from $T_{Air}$, like in Halle, where only 66.8 % of the time $T_{UCP}$ exceeds $T_{Air}$.

The average regression of all UCPs (y = 0.42× + 13, $r$ = 0.78) is in line with the findings of Rotta Loria et al. (2022), who also report a positive linear relation (y = 0.6× + 10.2, $r$ = 0.75) between $T_{UCP}$ and $T_{Air}$. The steeper gradient indicated that the UCPs in Chicago are better connected to surface air and adjust better to $T_{Air}$. This may be caused by differences in construction or higher ventilation. Note that in contrast to our approach, Rotta Loria et al. (2022) computed the regression for all UCPs at once using local above-ground air temperature data and within the same period. In this study, a regression is calculated for each individual data set, temperatures are recorded at variable times, and $T_{Air}$ is taken from meteorological monitoring that is typically located in the outskirts of the city. Applied to our data, the correlation coefficient would be weaker if calculated for all available data ($r$ = 0.65). The average regression lines of the respective levels, which are also shown in the bottom plot in Fig. 5, show a decreasing correlation coefficient with increasing level. In particular, the first level, which has a correlation coefficient of $r$ = 0.84, seems to respond well to $T_{Air}$ change. However, it should be noted, that the number of measurements decreases with increasing level as there are fewer UCPs with three or more levels available.

A source of the heat in UCPs seems to be the frequently parked cars. Especially at public UCPs, parked cars are often replaced several times a day, and heat from the engines of the parked cars warms the UCP (Becker and Epting, 2021). This is also clearly visible in Fig. 6, where the bar plots on the right show the daily average $T_{UCP}$ at all sites. While private UCPs are generally warmer during working days, the public ones gradually get warmer with each working day until Friday. They then significantly cool down on Sundays due to the reduced traffic. Becker and Epting (2021) made the same observation for the UCPs in Basel and also showed this effect for public holidays. In addition, the weekly averaged time series of $T_{UCP}$ is plotted on the left. The private UCPs are on average 16.6 ± 5.1 °C warm, while the public UCPs are 19.5 ± 4.6 °C warm. The mean $T_{UCP}$ of all studied sites is 18.8 ± 4.9 °C. Private UCPs typically have fewer levels and car exchange, which may be the reason for lower $T_{UCP}$ in comparison to public UCPs. The locations of the UCPs may influence the results as well. Public UCPs are often located in the city centers, where $T_{Air}$ is typically higher than in residential areas, in which private UCPs are commonly found.

Fig. 7 shows violin plots of the temperature difference between $T_{UCP}$ and $T_{Air}$ for each level. At all sites, $T_{UCP}$ is warmer than $T_{Air}$ on a long-term average and the temperature difference increases towards deeper levels. In particular, there is a significant increase of 2.8 K in the temperature difference between the first and second level. Furthermore, at the first level, almost 25 % of all values are negative, showing that $T_{UCP}$ is colder than $T_{Air}$ at these times. However, less data is available at deeper levels and additional data from deeper UCPs is needed to validate the observations.

The comparison of $T_{UCP}$ and $T_{Air}$ also shows that, particularly in the winter season, UCPs are warmer than the outside air. The deeper, public UCPs, such as Cologne #8, Basel #4, and #5, have $T_{UCP}$ continuously

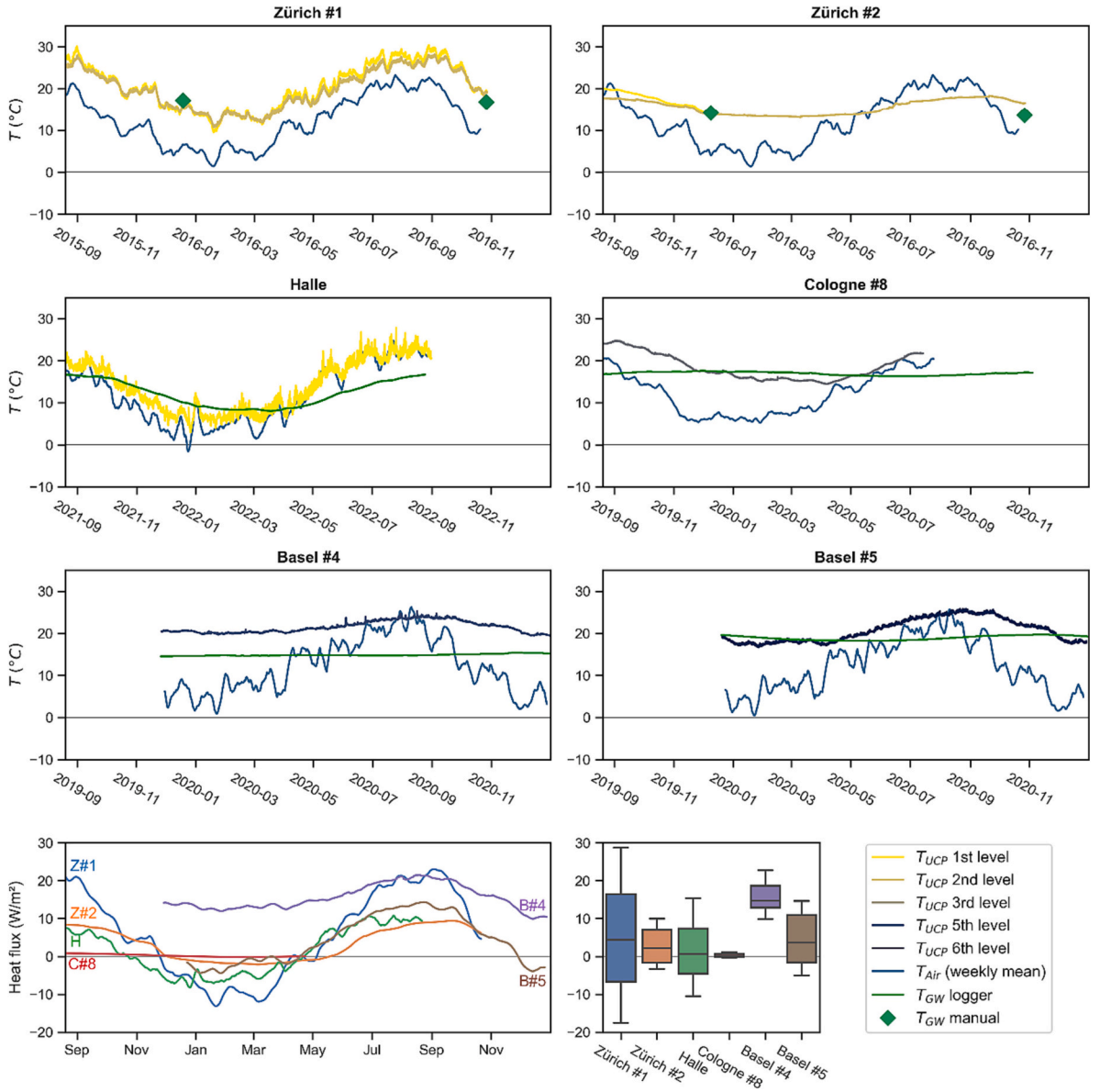


**Fig. 4.** Time series of groundwater temperature ($T_{GW}$), UCP temperature ($T_{UCP}$), and surface air temperature ($T_{Air}$) for six UCPs as well as temporally resolved heat fluxes through the slab into the groundwater.

>15 °C in the winter season, as seen in Fig. 4. This suggests that UCP air could itself be a sustainable energy source. I.e., integrating heat pumps in existing ventilation systems might be a way to utilize waste heat energy from UCP air. Harnessing this potential can supply nearby residential or commercial buildings with sustainably generated heat energy and, at the same time, reduce the thermal impact on the subsurface.

### 3.2. Impact of underground car parks on subsurface warming of Berlin

#### 3.2.1. Spatial and seasonal analysis of heat fluxes

The heat flux from UCPs in Berlin exhibits a high spatial variance that is mainly driven by the distance to the groundwater, local $T_{GW}$, and for the accumulated heat fluxes the density of UCP per area. Principle statistics of the UCP heat flux for each city district are provided in the Appendix in Table A3. In total, 0.7 % of the study area is covered by 5040 UCPs that produce an average heat flux through slab and walls of 3.7 W/m$^2$. The highest density of UCPs per surface area is found in the districts of Mitte (3.6 %) and Friedrichshain-Kreuzberg (3.5 %), with all other districts being lower than 1.5 %, down to 0.1 % in Reinickendorf.

The distance to the groundwater is tightly linked to geological features and is the major controlling factor for the heat flux (Fig. 8a). In the glacial valley the groundwater distance is typically below 10 m and a high fraction of UCPs are in direct contact with groundwater (up to 35 % in Treptow-Köpenick). The two districts with the highest UCP density, Mitte and Treptow-Köpenick, are also in the valley region and have the highest heat fluxes at 4.8 and 6.8 W/m$^2$, respectively. In Mitte, 21.4 % of the heat flux is through the walls due to the high groundwater levels. In Treptow-Köpenick, only 2.9 % of the heat emits through walls, although 35.1 % of the UCPs are in contact with groundwater. This is because, in contrast to Mitte, the UCPs in Treptow-Köpenick typically have fewer levels and do not reach as deep in the groundwater. Still, heat fluxes in Mitte are on average lower than in Treptow-Köpenick because of the higher $T_{GW}$ in the city center which result in a lower thermal gradient. Likewise, the districts of Spandau, Reinickendorf, and Friedrichshain-Kreuzberg are also located in the glacial valley and therefore have comparably high heat fluxes between 3.8 and 4.2 W/m$^2$. On the Teltow (southwest) and Barnim (northeast) plateaus the distance to groundwater is typically above 10 m and in districts that are exclusively on the

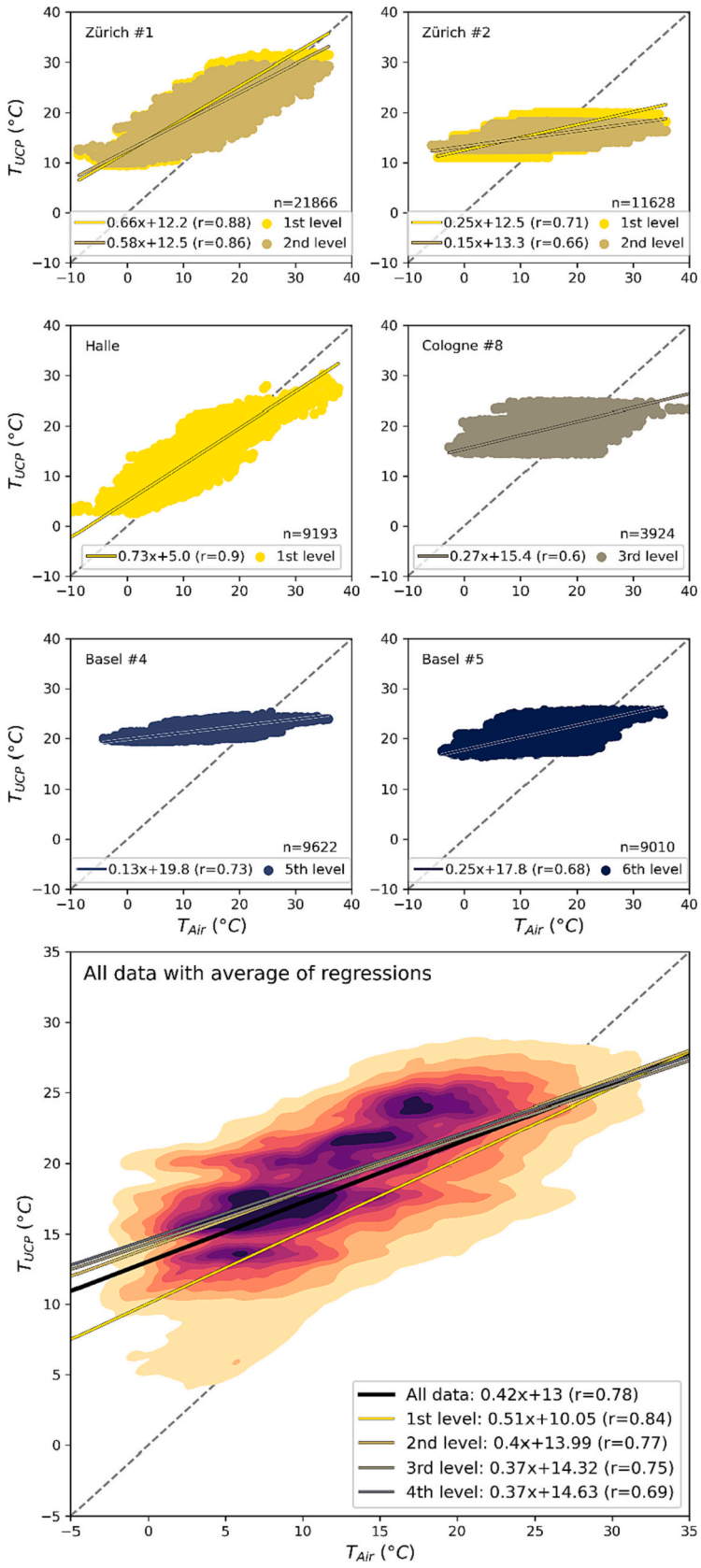


**Fig. 5.** UCP temperature ($T_{UCP}$) and surface air temperature ($T_{Air}$) correlation for six selected sites. The colors indicate the level of the UCP at which the measurement was taken. The bottom diagram contains the data for all 31 sites and the average of the results of each individual regression for the respective levels. All plots have a dashed identity line as reference. The number of measurements is marked with an n.

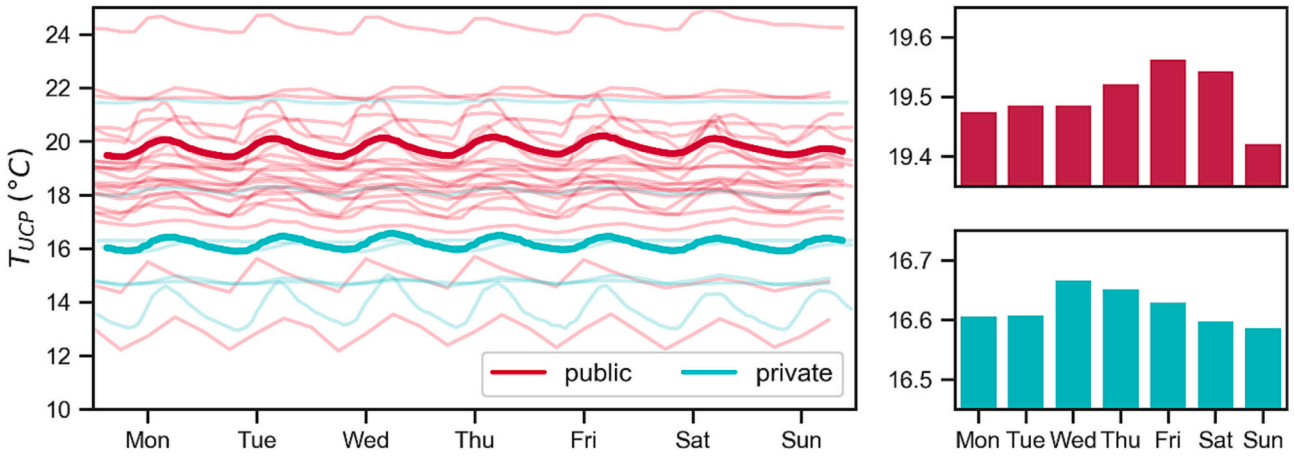


**Fig. 6.** Weekly averaged time series of the UCP temperature ($T_{UCP}$) and daily mean values for public (red) and private (green) UCPs. Thick lines represent a rolling mean (6 h) of all publicly and privately studied sites.

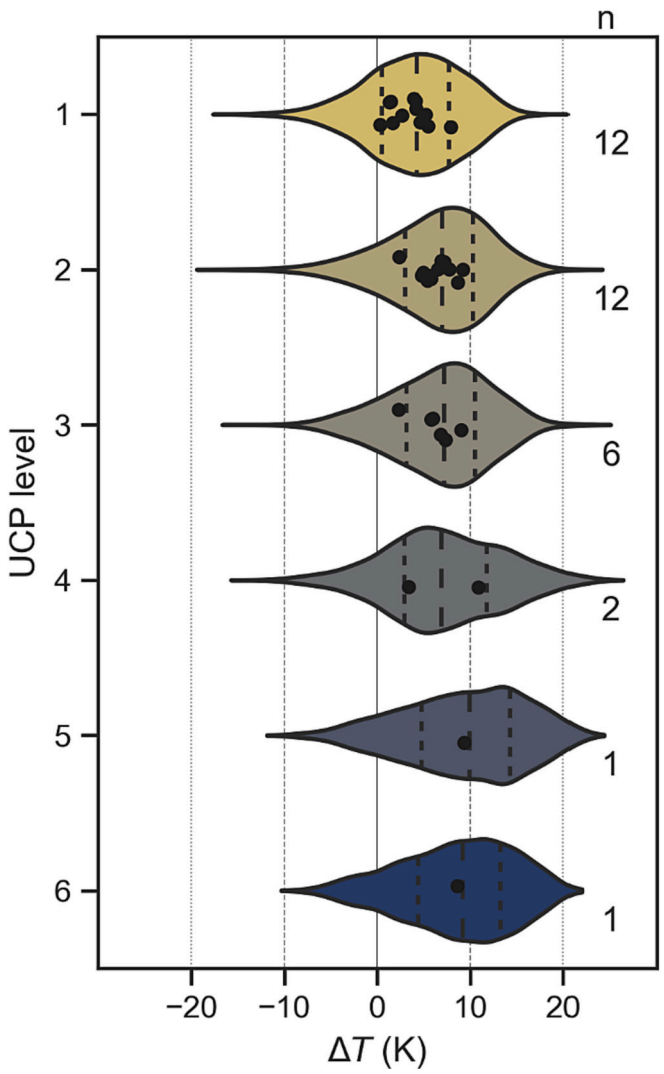


**Fig. 7.** Violin plots of the temperature difference ($\Delta T$) between UCP and surface air at each level. The dots represent mean values of the individual UCPs. The number of UCPs is marked with an n.

plateaus like Steglitz-Zehlendorf UCPs are not in direct contact with groundwater. Consequently, those UCPs which are on the plateaus have low heat fluxes <1 W/m$^2$.

For the sum of the heat flows from all UCPs per city quarter the UPC density and size are the dominant factors and groundwater depth and temperature play a subordinate role (Fig. 8b.) The by far highest overall impact on $T_{GW}$ occurs in Mitte with 8.2 MW and 259.5 TJ of heat energy emitted annually into the groundwater, which corresponds to 40 % of the total heat flow of Berlin (20.7 MW; 652.6 TJ/a). Marzahn-Hellersdorf on the other hand has the lowest number of UCPs (122), which results in the smallest total heat flow of <0.1 MW and 3.2 TJ per year.

The heat flux through the UCP slab and walls shows a strong seasonal behavior in response to the seasonal oscillation of $T_{UCP}$ (Fig. 9). While all UCPs heat the groundwater between April and October, differences in thermal behavior are observed for March and November. In particular in regions with high $T_{GW}$ like the city center UCPs cool the surrounding subsurface. In the winter months, between December and February, about 75 % of the UCPs cool the groundwater. Conversely, this means that the remaining 25 % of UCPs heat the groundwater all year round. The annual average shows that 76 % of the UCPs have a heat flux between 0 and 5 W/m$^2$. However, some outliers appear to be highly effective heat sources with an average heat flux of 17 W/m$^2$ and up to 26.3 W/m$^2$ in July. These UCPs are located in Mitte close to the Spree River and urban green areas, where groundwater levels are relatively high and $T_{GW}$ cool (11–12 °C). Considering a full annual cycle, all UCPs in Berlin have a net positive heat flux and therefore act as heat sources for the groundwater.

The heat fluxes of the measured UCPs are in line with the spatial analysis for Berlin. Five of the six reference UCPs seen in Fig. 4 also have an average heat flux between 0 and 5 W/m$^2$. With Basel #4, we have identified a UCP that is similar to the positive outliers in the spatial analysis and acts as a highly effective heat source throughout the year. The mean heat flux of the six sites presented in the UCP temperature analysis (Fig.) is 4.8 W/m$^2$, which is higher than the mean value of the UCPs in Berlin (3.2 W/m$^2$). This is because the six measured sites, with the exception of Cologne #8, all have a very small distance to the groundwater of 0.5 m or less.

To address the parameter sensitivity of this approach additionally to Table A4, where the uncertainties of the spatial analysis are given, we applied the minimum and maximum values for each assumed parameter from Table A2 one at a time and show the error ranges in Fig. A4. The most sensitive parameters appear to be $T_{UCP}$ and $T_{GW}$, as a variation of 1 K changes the mean $q_{slab+wall}$ from 3.7 to 2.6 W/m$^2$. Furthermore, the thermal conductivity of concrete has a high sensitivity, especially the lower-end value of 0.9 W/m·K reduces the mean $q_{slab+wall}$ to 2.5 W/m$^2$.

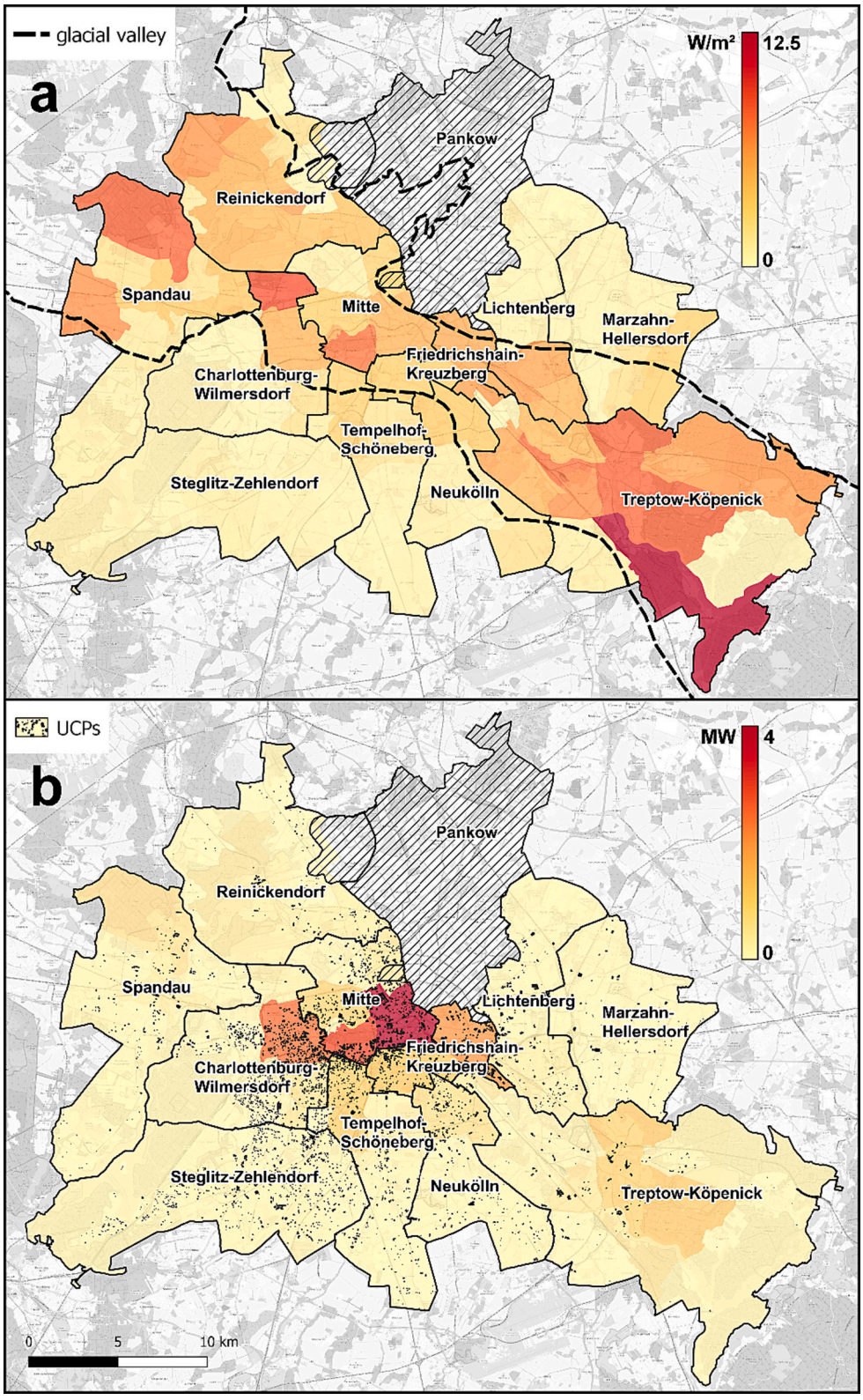


**Fig. 8.** **(a)** Map of Berlin showing the mean heat flux through slabs ($q_{slab}$) into the groundwater per city quarter. The dashed line shows the approximate boundary of the glacial valley. **(b)** Map of the total heat flow ($Q$) from UCPs into the groundwater per city quarter. The black polygons represent the UCPs. Districts are labeled and delimited with black lines. Hatched areas have insufficient data. Background map source: OpenStreetMap.

This shows the high impact insulation of the slab can have on the heat losses to the ground.

### 3.2.2. Relation to other studies and heat sources

Tissen et al. (2021) determined a heat flow from various sources as a heat supply rate for shallow geothermal units for a city quarter in Vienna, Austria. They determined a total heat flow of 0.02 ± 0.01 PJ/a

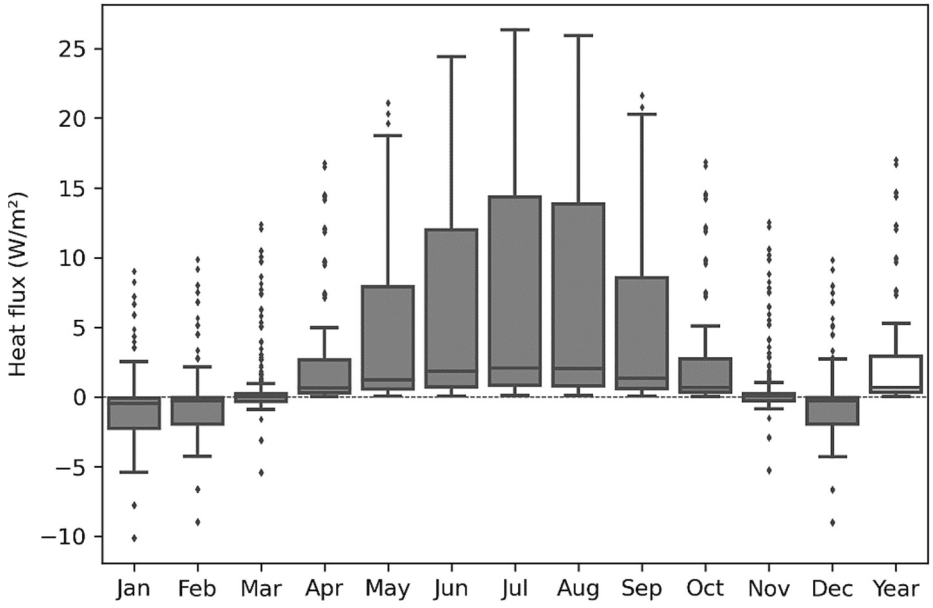


**Fig. 9.** Monthly heat flux through slab and wall and average annual heat flux from each UCP in Berlin ($n$ = 5040).

from UCPs in Vienna based on 12 UCPs. In comparison, the impact from UCPs in Berlin is much larger at 0.65 PJ/a which accumulates from 5040 UCPs. As the total numbers are not comparable based on the number of UCPs considered, a better comparison can be made based on the average heat flux from UCPs. Tissen et al. (2021) calculated a mean value of 15.4 ± 5.2 W/m$^2$, which is significantly larger than in Berlin with 3.7 ± 2.2 W/m$^2$. This discrepancy could be caused by a different approach in the heat flux calculation. Tissen et al. (2021) used Fourier's laws to calculate the conductive heat transport between groundwater and UCP air, but do not consider the thermal properties of the slab and heat transfer coefficients.

Becker and Epting (2021) show mean heat fluxes of 0.3–4.0 W/m$^2$ for 5 UCPs in Basel. They used the same sites that are also used in this study but found noticeably smaller heat fluxes for the UCPs of Basel #4 (0.5 vs. 4.3 W/m$^2$) and Basel #5 (4.0 vs. 15.5 W/m$^2$). This discrepancy is caused by different values for the thermal transmittance of the UCP wall. Becker and Epting (2021) calculated with insulated UCPs, whereas in this study we assume that walls and slabs in UCPs are not insulated, since UCPs are generally unheated rooms and insulation is not legally required in Germany (§2 GEG, 2020). Hence, the thermal transmittance in our study for the same UCPs is higher than in Becker and Epting (2021). This discrepancy also shows the magnitude of impact an insulation of UCPs and basements has on mitigating heat losses into the ground.

Benz et al. (2015), who generalized the anthropogenic heat flow for all buildings and basements in Karlsruhe and Cologne, found impacts of 1.5 ± 1.4 PJ/a and 0.3 ± 0.1 PJ/a, respectively. The reason for the low heat flow in Cologne is the high distance to groundwater. The resulting small heat fluxes were also observed for the UCP Cologne #8 in Fig. 4. The heat flow of UCPs in Berlin is more than double (0.65 PJ/a) than in Cologne. This amount of energy corresponds to the heating demand of 14,660 average German households, or 29,639 people, respectively (Destatis, 2023).

Compared to the heat flux induced by earth's energy imbalance due to atmospheric warming, which is 550–890 mW/m$^2$ for the period 1993–2018 (Forster et al., 2021), the heat emission of Berlin's UCPs is with an average $AHF_{UCP}$ of 26.7 mW/m$^2$ still relatively low. However, the terrestrial heat flux is about 67.1 mW/m$^2$ (Lucazeau, 2019), which is exceeded by the $AHF_{UCP}$ in the districts of Mitte (214.5 mW/m$^2$) and Friedrichshain-Kreuzberg (148.2 mW/m$^2$), where the heat flux normalized to the area of the district is highest due to the high UCP density. In the district of Marzahn-Hellersdorf, on the other hand, we found both a low number of UCPs (122) and a high distance to groundwater, resulting in the lowest $AHF_{UCP}$ of 1.6 mW/m$^2$. Considering that other heat sources, such as sewer and district heating pipes, tunnels, and surface sealing, yield an additional anthropogenic impact on subsurface temperatures, urban subsurface warming trends are expected to increase, resulting in rising $T_{GW}$ in cities.

In comparison to the thermal impact of other structures, UCPs create stronger local anomalies but have a smaller overall contribution to subsurface warming. For example, our findings of the average heat flux from UCPs in Berlin (3.7 ± 2.2 W/m$^2$) are higher than the heat fluxes from basements in Basel (0.20–0.89 W/m$^2$), numerically modeled for different settings (Epting et al., 2017a), or in Winnipeg, Canada, with ~2 W/m$^2$ (Ferguson and Woodbury, 2004). The normalized heat flux per area, however, is typically higher for basements and buildings as the area covered by these heat source types is larger. Compared to the low $AHF_{UCP}$ of 26.7 mW/m$^2$ in Berlin, the AHF of buildings in Osaka, Japan, is one order of magnitude greater with 320 ± 180 mW/m$^2$ (Benz et al., 2018) and two orders of magnitude in Basel (5900 to 8000 mW/m$^2$) (Mueller et al., 2018).

Thermal alteration of groundwater is assumed to impact groundwater ecology and quality (Becher et al., 2022). In Berlin, special attention must be paid to areas in the Warsaw-Berlin glacial valley when it comes to groundwater protection since areas of small groundwater depth are most vulnerable to thermal pollution of aquifers (Blum et al., 2021). However, a moderate increase in $T_{GW}$ of 5 to 10 K yields only a minor impact on groundwater chemistry, microbiology, and fauna (Griebler et al., 2016). To date, only local thermal anomalies of highly effective heat sources (e.g., power plants or landfills) or accumulations of heat sources in dense urban areas exceed these limits. Nonetheless, mitigation of high $T_{GW}$ by extracting heat with geothermal applications not only protects groundwater ecosystems and urban freshwater resources but also has the potential to sustainably supply local infrastructure and buildings with green energy (Epting et al., 2020). The heated urban environment therefore benefits geothermal applications economically in contrast to a cooler rural setting. So-called energy geostructures, which integrate heat exchanger in foundations of buildings, might be a solution for harnessing subsurface waste heat in areas of limited available space (Brandl, 2006; Loveridge et al., 2020). For example, heat exchanger can be implemented in the slab of an UCP (Lee et al., 2023). In comparison to unheated basements, publicly used UCPs

have particularly high indoor temperatures and hence high local impacts on $T_{GW}$, which increases the efficiency of geothermal heat pumps. However, an increasing number of geothermal applications in cities raises the need of managing geothermal potential (Attard et al., 2020; Epting et al., 2017a; García-Gil et al., 2020).

While the methods can be applied to any urban area as it accounts for climatic and hydrogeological parameters, the results of this study should not be generalized to other settings. For example, Mediterranean cities have higher natural $T_{GW}$ and *TAir* and therefore different environmental conditions and energy demands. Recycling of waste heat is only meaningful when the heating demand is high.

## 4. Conclusions

In this study, we investigated the thermal impact of underground car parks (UCPs) on groundwater. For this purpose, we collected data from 31 sites in Germany, Austria, and Switzerland. The dataset includes time series of $T_{UCP}$, $T_{Air}$, and at six sites $T_{GW}$. In order to evaluate the impact on a regional scale, we expanded our analysis to 5040 UCPs in Berlin, Germany, and assessed the patterns and influencing factors of their heat fluxes.

We found the mean $T_{UCP}$ on all investigated sites to be 18.8 ± 4.9 °C. However, $T_{UCP}$ varies significantly from site to site based on the depth and usage type of the UCP. We identified cars to be a potential driver of $T_{UCP}$, as public UCPs, which generally have more traffic, are on average 2.9 K warmer than private UCPs. In addition, we observed that $T_{UCP}$ is cooler on Sundays when the traffic is reduced. Towards deeper levels the deviation between $T_{Air}$ and $T_{UCP}$ increases. For example, the temperature difference at the second level is on average 2.8 K higher than in the first level and subsequently hotter in the levels below. The evaluation of repeated recordings of temperature-depth-profiles confirms our understanding that public UCPs yield a higher impact on $T_{GW}$ than private ones. All six sites with $T_{GW}$ time series can be considered as net heat sources, with their heat fluxes into the groundwater ranging between 0.3 and 15.5 W/m$^2$ and seasonal variations in intensity and direction. For the UCP of Basel #4, which has the largest impact, we detected temporally continuous heat fluxes of >10 W/m$^2$. Finally, we computed the mean of the individual linear regression from all sites to be able to derive $T_{UCP}$ from $T_{Air}$ to upscale the effect UCPs have at the city-scale.

Together with other open data, the regressions were used to estimate the $T_{UCP}$ of 5040 UCPs in Berlin. The average heat flux from UCP slabs into the groundwater in the study area is 3.2 W/m$^2$. However, if the walls within the saturated zone are considered, the rate increases to 3.7 W/m$^2$. The average $AHF_{UCP}$ of UCPs in Berlin is 26.7 mW/m$^2$, which is still lower than the heat flux induced by atmospheric warming (550–890 mW/m$^2$) and the terrestrial heat flux (67.1 mW/m$^2$). The district of Mitte has the highest impact with an $AHF_{UCP}$ of 214.5 mW/m$^2$ and a total heat flow of 8.2 MW, which corresponds to 40 % of the total heat flow of Berlin (20.7 MW). This is due to the high UCP density and shallow groundwater in Mitte and despite the already heated groundwater. Besides the density and size of UCPs, we determined the shallow (hydro-)geological conditions as the driving factor for the distribution of heat flows. On the Barnim and Teltow plateaus in the northeast and southwest of Berlin, heat fluxes are typically lower than in the Warsaw-Berlin glacial valley (southeast to northwest). Therefore, we identified the glacial valley as most vulnerable to thermal pollution. On the other hand, the higher $T_{GW}$ likewise enables higher efficiency of geothermal applications that utilize subsurface waste heat. Furthermore, harnessing the heat energy that is retained in UCP air through heat pumps in existing ventilation systems might be another solution for generating sustainable energy while reducing the thermal footprint on the subsurface. When looking at the individual UCPs in Berlin, we found that all UCPs heat the groundwater between April and October and the majority (about 75 %) cool the groundwater between December and February. On an annual average, all UCPs in Berlin act as heat source. Ultimately, 652.6 TJ of thermal energy is emitted into the groundwater in the study area annually. This amount of energy is equivalent to the heating demand of 14,660 average German households or 29,639 people, respectively.

## CRediT authorship contribution statement

**Maximilian Noethen:** Conceptualization, Methodology, Validation, Formal analysis, Data curation, Writing – original draft, Visualization. **Hannes Hemmerle:** Conceptualization, Resources, Writing – review & editing. **Kathrin Menberg:** Resources, Writing – review & editing. **Jannis Epting:** Resources, Writing – review & editing. **Susanne A. Benz:** Resources, Writing – review & editing. **Philipp Blum:** Resources, Writing – review & editing. **Peter Bayer:** Conceptualization, Writing – review & editing, Supervision, Funding acquisition.

## Declaration of competing interest

The authors declare that they have no known competing financial interests or personal relationships that could have appeared to influence the work reported in this paper.

## Data availability

Data will be made available on request.

## Acknowledgements

The financial support for Maximilian Noethen from the Scholarship Programme of the German Federal Environmental Foundation (DBU) is gratefully acknowledged. Also, the financial support for Kathrin Menberg via the Margarete von Wrangell program of the Ministry of Science, Research and the Arts (MWK) of the State of Baden-Württemberg is gratefully acknowledged. We would also like to thank Cathrin Dreher (Senatsverwaltung für Umwelt, Verkehr und Klimaschutz), Rudolf Hunold and Stefan Schiffmann (RheinEnergie AG), Roger Wismer (Schutz und Rettung Zürich) as well as Ulrike Thies (freelance architect) for their valuable support with data and additional information. Further, we thank the Office for Environment and Energy, Canton Basel-Stadt (AUE-BS) for providing data. We would also like to express gratitude towards Carolin Tissen, Dominic Becker, and Julia Becher for providing data and help. We thank Ryan Pearson for language editing. Furthermore, we would like to thank David Hoffmann for his technical support during the data collection.

## Appendix A. Appendix

**Table A1**
Information and datasets used for the UCP temperature analysis.

| Name | Depth of structure (m) | No. of levels | Type of use | Device | Measuring period | Temporal resolution (h) | Assigned weather station | Distance to weather station (km) | Well distance (m) |
|---|---|---|---|---|---|---|---|---|---|
| Basel #1 | 9 | 2 | Public | EA WLAN-TH+ | 2019/12–2020/12 | 1 | BKLI, BAES[a] | 2.1 | – |
| Basel #2 | 11.3 | 3 | Public | | | 1 | | 2.2 | – |

(*continued on next page*)

**Table A1** (*continued*)

| Name | Depth of structure (m) | No. of levels | Type of use | Device | Measuring period | Temporal resolution (h) | Assigned weather station | Distance to weather station (km) | Well distance (m) |
|---|---|---|---|---|---|---|---|---|---|
| Basel #3 | 8.6 | 3 | Public | | | 1 | | 0.6 | – |
| Basel #4 | 11.3 | 5 | Private | | | 1 | | 1.1 | 130 |
| Basel #5 | 17.9 | 7 | Public | | | 1 | | 0.2 | 150 |
| Cologne #1 | 3.1 | 1 | Public | DS1922L iButton | 2019/03–2020/08 | 1 | Köln-Stammheim[b] | 5.6 | – |
| Cologne #2 | 3.2 | 1 | Public | | | 1 | | 7.4 | – |
| Cologne #3 | 5.6 | 2 | Public | | | 1 | | 6.3 | – |
| Cologne #4 | 5.9 | 2 | Public | | | 1 | | 5.3 | – |
| Cologne #5 | 5.4 | 2 | Public | | | 1 | | 6 | – |
| Cologne #6 | 5.7 | 2 | Public | | | 1 | | 5.7 | – |
| Cologne #7 | 6.4 | 2 | Public | | | 1 | | 5.1 | – |
| Cologne #8 | 8.4 | 3 | Public | | | 1 | | 6 | 10 |
| Cologne #9 | 11.5 | 4 | Public | | | 1 | | 6.3 | – |
| Cologne #10 | 10.6 | 4 | Public | | | 1 | | 5.5 | – |
| Halle | 3.5 | 1 | Private | HOBO MX2201 | 2021/08–2022/08 | 1 | Heide-Süd[c] | 1.8 | 35 |
| Karlsruhe | 3 | 1 | Private | HOBO MX100 | 2018/06–2022/07 | 3 | Rheinstetten[b] | 7.1 | – |
| Vienna #1 | 3[f] | 1 | Public | DS1922L | 2018/ | 6 | Hohe Warte[d] | 7.8 | – |
| Vienna #2 | 3[f] | 1 | Public | iButton | 04–2019/06 | 6 | | 8.5 | – |
| Vienna #3 | 3[f] | 1 | Public | | | 6 | | 10.1 | – |
| Vienna #4 | 3[f] | 1 | Private | | | 6 | | 5.8 | – |
| Vienna #5 | 3[f] | 1 | Private | | | 6 | | 12.4 | – |
| Vienna #6 | 3[f] | 1 | Private | | | 6 | | 12.6 | – |
| Vienna #7 | 6[f] | 2 | Public | | | 6 | | 6.5 | – |
| Vienna #8 | 6[f] | 2 | Public | | | 6 | | 4.3 | – |
| Vienna #9 | 6[f] | 2 | Public | | | 6 | | 11.1 | – |
| Vienna #10 | 9[f] | 3 | Public | | | 6 | | 5.3 | – |
| Vienna #11 | 9[f] | 3 | Public | | | 6 | | 7.4 | – |
| Vienna #12 | 9[f] | 3 | Public | | | 6 | | 7.5 | – |
| Zürich #1 | 9.2 | 3 | Public | DS1922L | 2014/ | 2 | Schimmel-straße[e] | 1.3 | 0 |
| Zürich #2 | 16.1 | 4 | Private | iButton | 12–2016/10 | 2 | | 1.1 | 0 |

[a] Research group Meteorology, Climatology and Remote Sensing, University of Basel
[b] DWD (2023).
[c] Institute of Geosciences and Geography, Martin Luther University Halle-Wittenberg.
[d] ZAMG (2023).
[e] Stadt Zürich (2023).
[f] Assumed depth.

**Table A2**
List of input parameters applied in the spatial analysis.

| Name | Parameter | Unit | Minimum | Mode | Maximum |
|---|---|---|---|---|---|
| Thermal conductivity sand | $\lambda_{soil}$ | W/m·K | 0.4 | 0.9 | 1.4 |
| Thermal conductivity peat | | | 0.2 | 0.4 | 0.7 |
| Thermal conductivity till | | | 1.1 | 2.4 | 2.9 |
| Thermal conductivity concrete | $\lambda_{concrete}$ | | 0.9 | 1.6 | 2.0 |
| Groundwater temperature | $T_{GW}$ | °C | From Geoportal Berlin (2023) | | |
| UCP air temperature | $T_{UCP}$ | °C | Derived from $T_{Air}$, resolved by month and UCP level | | |
| UCP depth | $d_{UCP}$ | m | 2.5 | 3 | 3.5 |
| UCP slab thickness[a] | $d_{slab}$ | m | 0.4 | 0.5 | 0.6 |
| UCP wall thickness[a] | $d_{wall}$ | m | 0.2 | 0.3 | 0.4 |
| Soil thickness | $d_{soil}$ | m | From Geoportal Berlin (2023) | | |
| UCP area | $A_{UCP}$ | $m^2$ | From Geoportal Berlin (2023) | | |

[a] Minimum values were applied to calculate the maximum results and vice versa, as the thickness of a permeated layer is a resistance.

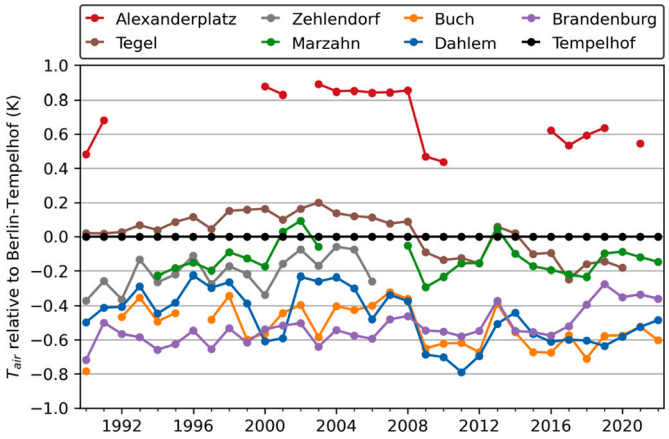


**Fig. A1.** Annual mean surface air temperature ($T_{Air}$) measured for eight weather stations in Berlin since 1990, relative to the weather station of Berlin-Tempelhof. Data source: DWD (2023).

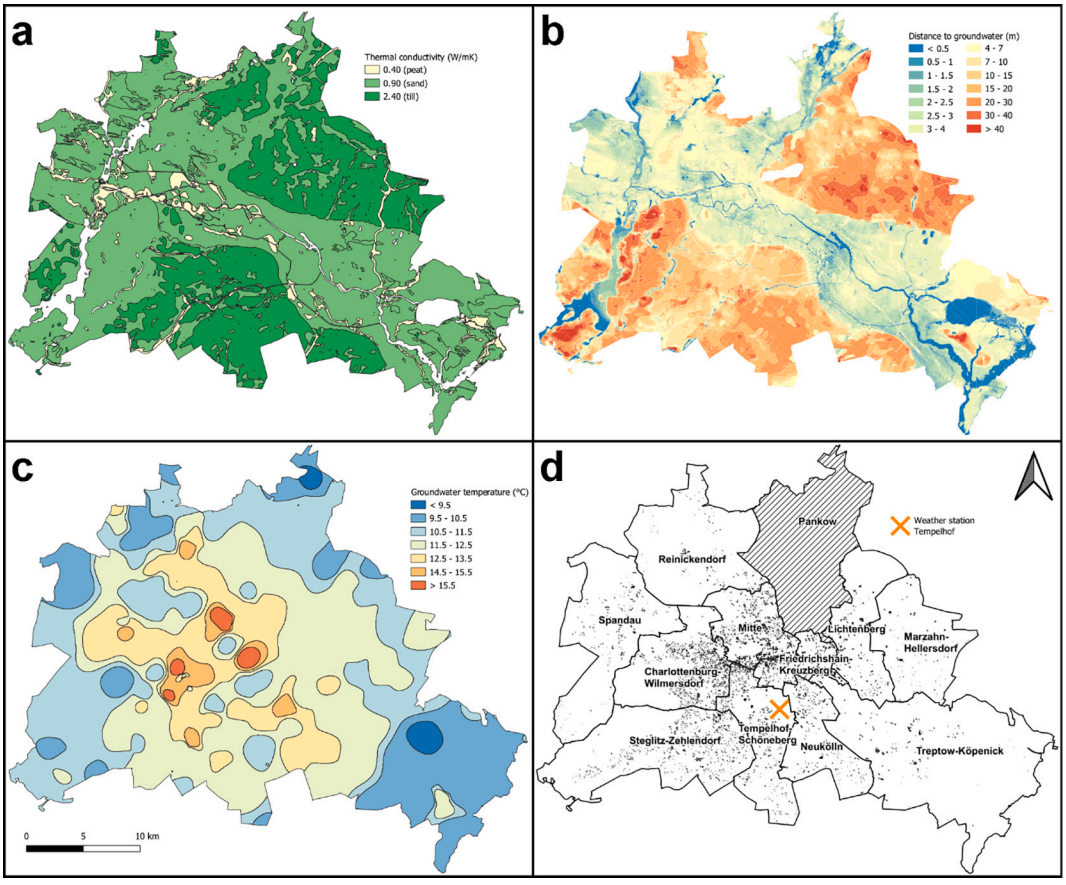


**Fig. A2.** Maps of Berlin showing the spatial datasets used as input for the analysis of the thermal impact of UCPs on the groundwater in Berlin. (a) Thermal conductivity of the shallow soil material. (b) Distance to the groundwater from the surface. (c) Groundwater temperature in 20 m below ground surface. (d) Shapes of UCPs, district areas, and location of the Tempelhof weather station.

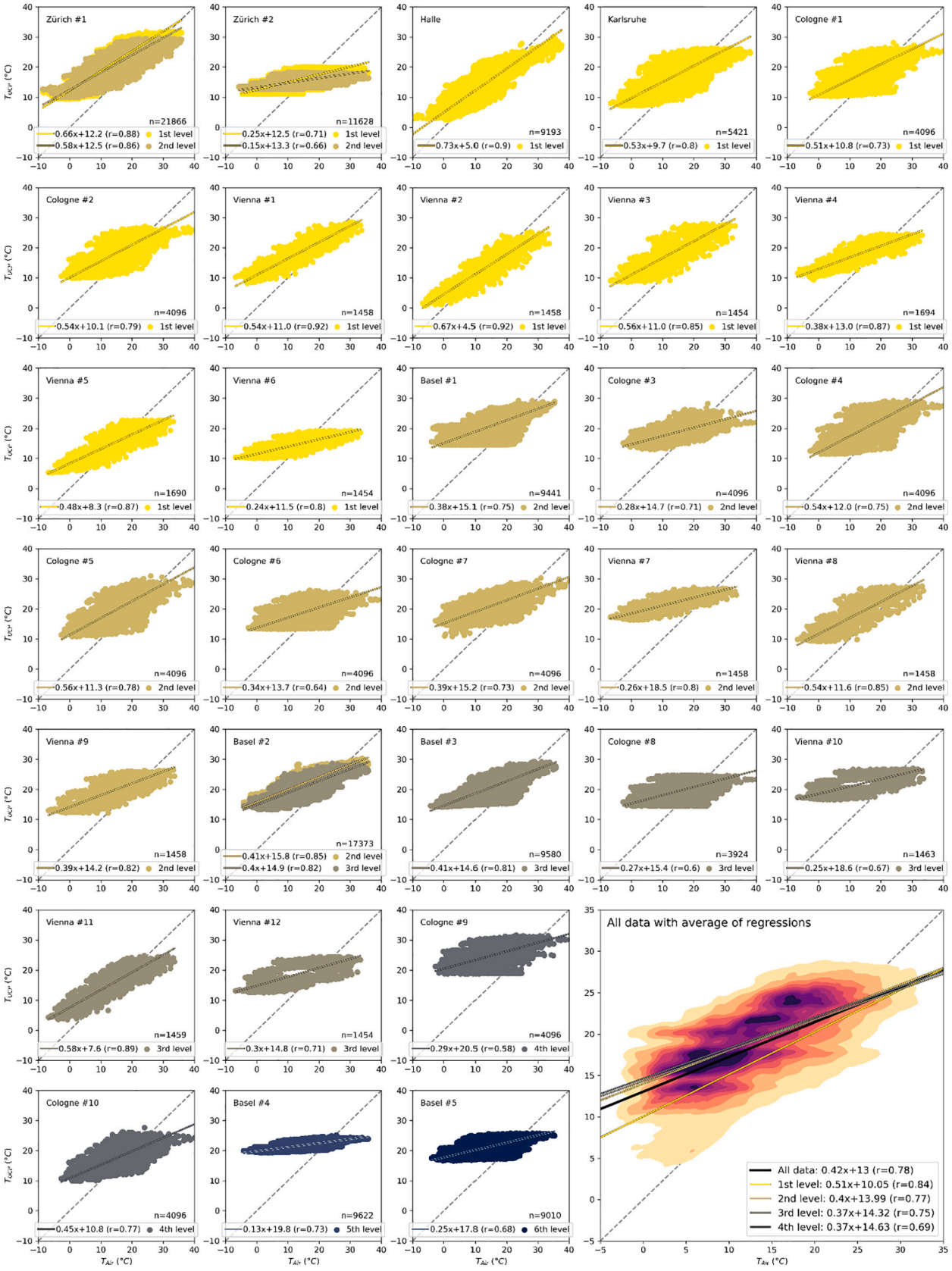


**Fig. A3.** Scatter plots for all 31 sites showing the correlation between UCP temperature ($T_{UCP}$) and surface air temperature ($T_{Air}$). The colors indicate the level of the UCP at which the measurement was taken. The bottom diagram contains the data for all 31 sites and the average of the results of each individual regression for the respective levels. All plots have a dashed identity line as reference. The number of measurements is marked with an n.

**Table A3**
Results of the spatial analysis of heat fluxes from UCPs in Berlin. Uncertainties of the results are shown in Table A4.

| District | Area ($km^2$) | UCP area ($km^2$) | Total UCPs (in GW) | Mean $q_{slab}$ ($W/m^2$) | Mean $q_{slab+wall}$ ($W/m^2$) | $AHF_{UCP}$ ($mW/m^2$) | Sum $Q$ (MW) | Yearly $E$ into GW (TJ/a) |
|---|---|---|---|---|---|---|---|---|
| Charlottenburg-Wilmersdorf | 64.7 | 1.0 | 1163 (82) | 2.8 | 3.2 | 48.0 | 3.1 | 98.0 |
| Friedrichshain-Kreuzberg | 20.2 | 0.7 | 349 (68) | 4.2 | 4.5 | 148.2 | 3.0 | 94.2 |
| Lichtenberg | 52.3 | 0.4 | 236 (28) | 1.8 | 1.8 | 13.1 | 0.7 | 21.6 |
| Marzahn-Hellersdorf | 61.7 | 0.2 | 122 (3) | 0.5 | 0.5 | 1.6 | <0.1 | 3.2 |
| Mitte | 38.4[a] | 1.4 | 881 (180) | 4.8 | 6.1 | 214.5 | 8.2 | 259.5 |
| Neukölln | 44.9 | 0.3 | 288 (26) | 2.0 | 2.1 | 13.7 | 0.6 | 19.4 |
| Reinickendorf | 78.2[a] | 0.1 | 169 (22) | 3.8 | 4.0 | 6.2 | 0.5 | 15.4 |
| Spandau | 91.9 | 0.2 | 227 (21) | 3.8 | 4.0 | 10.2 | 0.9 | 29.5 |
| Steglitz-Zehlendorf | 102.5 | 0.5 | 886 (0) | 0.5 | 0.5 | 2.5 | 0.3 | 8.1 |
| Tempelhof-Schöneberg | 53.1 | 0.6 | 528 (18) | 2.0 | 2.1 | 21.8 | 1.2 | 36.5 |
| Treptow-Köpenick | 168.4 | 0.3 | 191 (67) | 6.8 | 7.0 | 12.7 | 2.1 | 67.3 |
| Berlin | 776.4[a] | 5.5 | 5040 (515) | 3.2 | 3.7 | 26.7 | 20.7 | 652.6 |

[a] Areas without groundwater data are excluded (see Fig. A2 for comparison).

**Table A4**
Uncertainties of the spatial analysis, shown as minimum (min) and maximum (max) values.

| District | Mean $q_{slab}$ ($W/m^2$) | | Mean $q_{slab+wall}$ ($W/m^2$) | | $AHF_{UCP}$ ($mW/m^2$) | | Sum $Q$ (MW) | | Yearly E into GW (TJ/a) | |
|---|---|---|---|---|---|---|---|---|---|---|
| | Min | Max | Min | Max | Min | Max | Min | Max | Min | Max |
| Charlottenburg-Wilmersdorf | 1.5 | 3.7 | 1.6 | 4.7 | 24.4 | 70.0 | 1.6 | 4.5 | 49.9 | 142.9 |
| Friedrichshain-Kreuzberg | 2.2 | 5.6 | 2.3 | 6.3 | 77.8 | 210.3 | 1.6 | 4.2 | 49.4 | 133.6 |
| Lichtenberg | 0.9 | 2.4 | 0.9 | 2.5 | 6.8 | 18.1 | 0.4 | 0.9 | 11.2 | 29.9 |
| Marzahn-Hellersdorf | 0.3 | 0.7 | 0.3 | 0.7 | 0.8 | 2.1 | <0.1 | 0.1 | 1.6 | 4.2 |
| Mitte | 2.6 | 6.5 | 3.1 | 9.1 | 107.6 | 320.3 | 4.1 | 12.3 | 130.2 | 387.5 |
| Neukölln | 1.1 | 2.7 | 1.1 | 2.8 | 7.1 | 18.9 | 0.3 | 0.8 | 10.0 | 26.7 |
| Reinickendorf | 2.1 | 5.3 | 2.1 | 5.8 | 3.2 | 9.0 | 0.3 | 0.7 | 8.0 | 22.2 |
| Spandau | 2.0 | 5.3 | 2.1 | 5.7 | 5.3 | 14.5 | 0.5 | 1.3 | 15.5 | 42.0 |
| Steglitz-Zehlendorf | 0.3 | 0.7 | 0.3 | 0.7 | 1.2 | 3.2 | 0.1 | 0.3 | 3.7 | 10.4 |
| Tempelhof-Schöneberg | 1.0 | 2.6 | 1.1 | 2.9 | 11.1 | 29.8 | 0.6 | 1.5 | 18.5 | 49.9 |
| Treptow-Köpenick | 3.7 | 9.2 | 3.7 | 9.9 | 6.7 | 17.9 | 1.1 | 3.0 | 35.8 | 94.9 |
| Berlin | 1.7 | 4.4 | 1.9 | 5.4 | 13.6 | 38.6 | 10.6 | 29.9 | 333.8 | 944.1 |

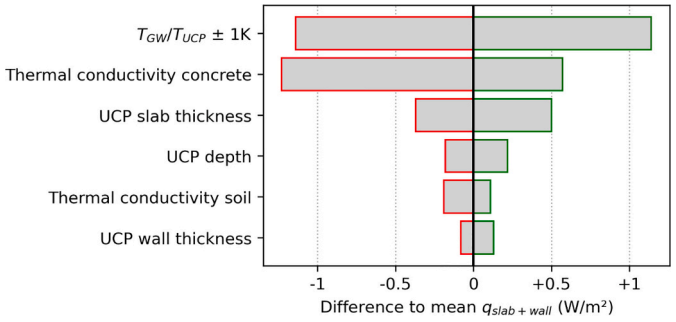


**Fig. A4.** Barplot showing the parameter sensitivity of the spatial analysis as difference to the mean $q_{slab+wall}$ of the total area of Berlin (3.7 $W/m^2$). The differences were calculated with only one parameter changed to the minimum and maximum values of Table A2.

## References

§11 GaVo, 2022. Garagenverordnung.
§2 GEG, 2020. Gebäudeenergiegesetz.
Agudelo-Vera, C., Avvedimento, S., Boxall, J., Creaco, E., de Kater, H., Di Nardo, A., Djukic, A., Douterelo, I., Fish, K.E., Iglesias Rey, P.L., 2020. Drinking water temperature around the globe: understanding, policies, challenges and opportunities. Water 12 (4), 1049.
Agudelo-Vera, C.M., Blokker, M., de Kater, H., Lafort, R., 2017. Identifying (subsurface) anthropogenic heat sources that influence temperature in the drinking water distribution system. Drink. Water Eng. Sci. Discuss. 10 (2), 83–91.
Attard, G., Rossier, Y., Winiarski, T., Eisenlohr, L., 2016. Deterministic modeling of the impact of underground structures on urban groundwater temperature. Sci. Total Environ. 572, 986–994.

Attard, G., Bayer, P., Rossier, Y., Blum, P., Eisenlohr, L., 2020. A novel concept for managing thermal interference between geothermal systems in cities. Renew. Energy 145, 914–924.
Becher, J., Englisch, C., Griebler, C., Bayer, P., 2022. Groundwater fauna downtown–drivers, impacts and implications for subsurface ecosystems in urban areas. J. Contam. Hydrol. 248, 104021.
Becker, D., Epting, J., 2021. Thermischer Einfluss urbaner Untergrundstrukturen auf die Grundwassertemperaturen im Kanton Basel-Stadt: Grundwasser, pp. 1–20.
Benz, S.A., Bayer, P., Menberg, K., Jung, S., Blum, P., 2015. Spatial resolution of anthropogenic heat fluxes into urban aquifers. Sci. Total Environ. 524, 427–439.
Benz, S.A., Bayer, P., Blum, P., Hamamoto, H., Arimoto, H., Taniguchi, M., 2018. Comparing anthropogenic heat input and heat accumulation in the subsurface of Osaka, Japan. Sci. Total Environ. 643, 1127–1136.
Benz, S.A., Menberg, K., Bayer, P., Kurylyk, B.L., 2022. Shallow subsurface heat recycling is a sustainable global space heating alternative. Nat. Commun. 13 (1), 3962.
Blum, P., Menberg, K., Koch, F., Benz, S.A., Tissen, C., Hemmerle, H., Bayer, P., 2021. Is thermal use of groundwater a pollution? J. Contam. Hydrol. 239, 103791.
Bonte, M., Stuyfzand, P., Van den Berg, G., Hijnen, W., 2011. Effects of aquifer thermal energy storage on groundwater quality and the consequences for drinking water production: a case study from the Netherlands. Water Sci. Technol. 63 (9), 1922–1931.
van den Bos, L., 2020. Quantifying the Effects of Anthropogenic Heat Sources on the Water Temperature in the Drinking Water Distribution System. TU, Delft.
Böttcher, F., Zosseder, K., 2022. Thermal influences on groundwater in urban environments–a multivariate statistical analysis of the subsurface heat island effect in Munich. Sci. Total Environ. 810, 152193.
Boulton, A.J., Fenwick, G.D., Hancock, P.J., Harvey, M.S., 2008. Biodiversity, functional roles and ecosystem services of groundwater invertebrates. Invertebr. Syst. 22 (2), 103–116.
Brandl, H., 2006. Energy foundations and other thermo-active ground structures. Géotechnique 56 (2), 81–122.
Brielmann, H., Griebler, C., Schmidt, S.I., Michel, R., Lueders, T., 2009. Effects of Thermal Energy Discharge on Shallow Groundwater Ecosystems.
Destatis, 2023. Statistisches Bundesamt. URL. https://www.destatis.de/DE/Themen/Gesellschaft-Umwelt/Umwelt/UGR/private-haushalte/Tabellen/raumwaerme-haushalte.html.
DIN EN ISO 6946, 2018. Bauteile - Wärmedurchlasswiderstand und Wärmedurchgangskoeffizient - Berechnungsverfahren.
Dugord, P.-A., Lauf, S., Schuster, C., Kleinschmit, B., 2014. Land use patterns, temperature distribution, and potential heat stress risk–the case study Berlin, Germany. Comput. Environ. Urban. Syst. 48, 86–98.
DWD, 2023. Climate Data Center. URL. https://cdc.dwd.de/portal/.
Emery, A., Heerwagen, D., Kippenhan, C., Steele, D., 2007. Measured and predicted thermal performance of a residential basement. HVAC&R Res. 13 (1), 39–57.
Epting, J., García-Gil, A., Huggenberger, P., Vázquez-Suñe, E., Mueller, M.H., 2017a. Development of concepts for the management of thermal resources in urban areas – assessment of transferability from the Basel (Switzerland) and Zaragoza (Spain) case studies. J. Hydrol. 548, 697–715.
Epting, J., Scheidler, S., Affolter, A., Borer, P., Mueller, M.H., Egli, L., García-Gil, A., Huggenberger, P., 2017b. The thermal impact of subsurface building structures on urban groundwater resources – a paradigmatic example. Sci. Total Environ. 596, 87–96.
Epting, J., Böttcher, F., Mueller, M.H., García-Gil, A., Zosseder, K., Huggenberger, P., 2020. City-scale solutions for the energy use of shallow urban subsurface resources – bridging the gap between theoretical and technical potentials. Renew. Energy 147, 751–763.
Ferguson, G., Woodbury, A.D., 2004. Subsurface heat flow in an urban environment. J. Geophys. Res. Solid Earth 109 (B2).
Forster, P., Storelvmo, T., Armour, K., Collins, W., Dufresne, J.-L., Frame, D., Lunt, D., Mauritsen, T., Palmer, M., Watanabe, M., 2021. The Earth's Energy Budget, Climate Feedbacks, and Climate Sensitivity.
García-Gil, A., Goetzl, G., Kłonowski, M.R., Borovic, S., Boon, D.P., Abesser, C., Janza, M., Herms, I., Petitclerc, E., Erlström, M., 2020. Governance of shallow geothermal energy resources. Energy Policy 138, 111283.
Geoportal Berlin, 2023. Senatsverwaltung für Stadtentwicklung, Bauen und Wohnen. URL. https://fbinter.stadt-berlin.de/fb/index.jsp.
Griebler, C., Avramov, M., 2015. Groundwater ecosystem services: a review. Freshwater Sci. 34 (1), 355–367.
Griebler, C., Brielmann, H., Haberer, C.M., Kaschuba, S., Kellermann, C., Stumpp, C., Hegler, F., Kuntz, D., Walker-Hertkorn, S., Lueders, T., 2016. Potential impacts of geothermal energy use and storage of heat on groundwater quality, biodiversity, and ecosystem processes. Environ. Earth Sci. 75 (20), 1–18.
Gunkel, G., Michels, U., Scheideler, M., 2022. Climate change: water temperature and invertebrate propagation in drinking-water distribution systems, effects, and risk assessment. Water 14 (8), 1246.
Guo, L., Guo, L., Zhong, L., Zhu, Y., 2011. Thermal conductivity and heat transfer coefficient of concrete. J. Wuhan Univ. Technol. Mater. Sci. Ed. 26 (4), 791–796.
Hancock, P.J., Boulton, A.J., Humphreys, W.F., 2005. Aquifers and hyporheic zones: towards an ecological understanding of groundwater. Hydrogeol. J. 13, 98–111.
Hannappel, S., Limberg, A., 2007. Ermittlung des Flurabstandes des oberflächennahen Grundwassers in Berlin (Determination of the floor distance of shallow groundwater in Berlin). Brandenburg Geowiss Beitr 14, 65–74.
Hemmerle, H., Ferguson, G., Blum, P., Bayer, P., 2022. The evolution of the geothermal potential of a subsurface urban heat island. Environ. Res. Lett. 17 (8), 084018.
Koch, F., Menberg, K., Schweikert, S., Spengler, C., Hahn, H.J., Blum, P., 2020. Groundwater fauna in an urban area: natural or affected? Hydrol. Earth Syst. Sci. Discuss. 1–23.
Kottmeier, C., Biegert, C., Corsmeier, U., 2007. Effects of urban land use on surface temperature in Berlin: Case study. J. Urban Plan. Dev. 133 (2), 128–137.
Lee, S., Park, S., Han, T.H., Won, J., Choi, H., 2023. Applicability evaluation of energy slabs installed in an underground parking lot. Sustainability 15 (4), 2973.
Limberg, A., Thierbach, J., 1997. Gliederung der Grundwasserleiter in Berlin. Brandenburgische Geowiss. Beitr 4 (2), 21–26.
Loveridge, F., McCartney, J.S., Narsilio, G.A., Sanchez, M., 2020. Energy geostructures: a review of analysis approaches, in situ testing and model scale experiments. Geomech. Energy Environ. 22, 100173.
Lucazeau, F., 2019. Analysis and mapping of an updated terrestrial heat flow data set. Geochem. Geophys. Geosyst. 20 (8), 4001–4024.
Menberg, K., Bayer, P., Zosseder, K., Rumohr, S., Blum, P., 2013a. Subsurface urban heat islands in German cities. Sci. Total Environ. 442, 123–133.
Menberg, K., Blum, P., Schaffitel, A., Bayer, P., 2013b. Long-term evolution of anthropogenic heat fluxes into a subsurface urban heat island. Environ. Sci. Technol. 47 (17), 9747–9755.
Menberg, K., Blum, P., Rivera, J., Benz, S., Bayer, P., 2015. Exploring the geothermal potential of waste heat beneath cities. In: Proceedings Proceedings World Geothermal Congress, pp. 1–5.
Mueller, M.H., Huggenberger, P., Epting, J., 2018. Combining monitoring and modelling tools as a basis for city-scale concepts for a sustainable thermal management of urban groundwater resources. Sci. Total Environ. 627, 1121–1136.
Noethen, M., Hemmerle, H., Bayer, P., 2022. Sources, intensities, and implications of subsurface warming in times of climate change. Crit. Rev. Environ. Sci. Technol. 1–23.
Oke, T.R., 1973. City size and the urban heat island. Atmos. Environ. (1967) 7 (8), 769–779.
Rotta Loria, A.F., Thota, A., Thomas, A.M., Friedle, N., Lautenberg, J.M., Song, E.C., 2022. Subsurface heat island across the Chicago Loop district: analysis of localized drivers. Urban Clim. 44, 101211.
Spengler, C., Hahn, H., 2018. Thermostress: Ökologisch gegründete, thermische Schwellenwerte und Bewertungsansätze für das Grundwasser (Ecological Based Temperature Thresholds and Ecosystem Assessment Schemes for Groundwater), 9. Korrespondenz Wasserwirtschaft, pp. 521–525.
Stadt Zürich, 2023. Open Data Zürich. URL. https://www.stadt-zuerich.ch/portal/de/index/ogd.html.
Thomas, H., Rees, S., 1999. The thermal performance of ground floor slabs - a full scale in-situ experiment. Build. Environ. 34 (2), 139–164.
Tissen, C., Menberg, K., Benz, S.A., Bayer, P., Steiner, C., Götzl, G., Blum, P., 2021. Identifying key locations for shallow geothermal use in Vienna. Renew. Energy 167, 1–19.
VDI 4640, 2010. Blatt 1: Thermal Use of the Underground, 33. VDI-Gesellschaft Energie und Umwelt, Düsseldorf.
Visser, P.W., Kooi, H., Bense, V., Boerma, E., 2020. Impacts of progressive urban expansion on subsurface temperatures in the city of Amsterdam (the Netherlands). Hydrogeol. J. 28 (5), 1755–1772.
Vogel, J., Afshari, A., 2020. Comparison of urban heat island intensity estimation methods using urbanized WRF in Berlin, Germany. Atmosphere 11 (12), 1338.
Ward, K., Lauf, S., Kleinschmit, B., Endlicher, W., 2016. Heat waves and urban heat islands in Europe: a review of relevant drivers. Sci. Total Environ. 569, 527–539.
ZAMG, 2023. GeoSphere Austria Data Hub. URL. https://data.hub.zamg.ac.at/.
Zhu, K., Bayer, P., Grathwohl, P., Blum, P., 2015. Groundwater temperature evolution in the subsurface urban heat island of Cologne, Germany. Hydrol. Process. 29 (6), 965–978.